PERGAMON

Deep-Sea Research II 49 (2002) 1441–1457

DEEP-SEA RESEARCH
PART II

www.elsevier.com/locate/dsr2

Water subducted into the Indian Ocean subtropical gyre ☆

Johannes Karstensen[a,*], Detlef Quadfasel[b]

[a] *Lamont-Doherty Earth Observatory of Columbia University, P.O. Box 1000, 61 Route 9W, Palisades, NY 10964-8000, USA*
[b] *Niels Bohr Institutet for Astronomi, Fysik og Geofysik, Geofysisk Afdeling og Center for Jordens Klima og Biogeokemiske Kredsløb, Københavns Universitet, Juliane Maries Vej 30, 2100 København Ø, Denmark*

Accepted 15 September 2001

Abstract

Subduction rates of the water into southern Indian Ocean permanent thermocline from 23.5 to 26.9 kg m^{-3} are calculated from a kinematic and a water-age approach and are compared with surface buoyancy flux calculations. The different estimates compare well within error margins, indicating that the effect of transient eddies on the subduction process is of second order. Considering only northward transport components, the overall transfer of water into the Indian Ocean thermocline is about 34 Sv (1 Sv = 10^6 m^3 s^{-1}), with equal contributions from lateral and vertical (essentially Ekman pumping) components. Ekman pumping dominates the upper density range (<25.2 kg m^{-3}), while for denser water the largest contribution stems from lateral input of Mode Waters. High silicate concentrations in the Mode Waters indicate that Southern Ocean waters participate in the formation process. The source water properties in salinity, oxygen, and nutrients along the surface of the deepest winter mixed layer are given.

1. Introduction

In the Indian Ocean the thermocline in both hemispheres is ventilated from the south, due to the absence of powerful sources in the north. The outflows from the arid Red Sea and the Arabian Gulf both inject highly saline waters into intermediate depth levels; however, their combined contribution including the entrained water is less then 2 Sv (Bower et al., 2000). The Pacific–Indian through flow imports water mainly in the upper part of the water column (Gordon et al., 1997) and the input in the permanent thermocline is marginal. In the northern Indian Ocean water-mass formation is limited to the winter monsoon season and to the northern Arabian Sea, ventilating only the upper thermocline at densities of about 24.0 kg m^{-3} at rates of less than 1 Sv over the whole year. It is rather the flow in the western boundary current off the African coast that leads to a renewal of the mid-depth waters in the northern Indian Ocean (Swallow, 1984). In this paper we estimate the flux rates into the thermocline of the southern subtropical gyre that have to supply also the northern hemisphere.

The permanent thermocline of the ocean is ventilated through subduction, the transfer of

☆ Lamont-Doherty Observatory Contribution number 6157.

*Corresponding author. Fax: +1-845-365-8155.
E-mail address: jkarsten@ldeo.columbia.edu (J. Karstensen).

0967-0645/02/$ - see front matter
PII: S0967-0645(01)00160-6

water from the near surface layer through the base of the mixed layer (Woods, 1985; Cushman-Roisin, 1987). Since this interface in general is not aligned horizontally, the flux across it is made up of a vertical and a horizontal component. Ekman pumping driven by the rotation of the wind field gives the vertical component (Iselin, 1939), whereas the horizontal velocity field gives the lateral component. The fluxes across the base of the mixed layer due to this horizontal flow depend of course strongly on the topography of the interface, which varies both in space and time (Woods, 1985; Marshall and Nurser, 1991; Williams et al., 1995). In particular transient eddies may contribute to this variability and thus to the overall subduction rates (Marshall, 1997).

Two different methods have been used to estimate subduction rates from observational data. The first is the "kinematic approach", based on the work of Woods (1985) and Cushman-Roisin (1987), that uses meteorological and hydrographic data and assumes geostrophy of the flow field (e.g. Marshall et al., 1993). The vertical component of the flux is derived from the curl of the wind-stress field, corrected for the forcing of the mixed layer itself (Williams, 1991). The lateral component is calculated using the topography of the deepest (winter) mixed-layer base and the velocity field at that depth (Fig. 1). The annual mean subduction rate S_{ann} can thus be written as

$$S_{\mathrm{ann}} = -w_{\mathrm{H}} + u_{\mathrm{H}} \cdot \nabla H(x, y). \quad (1)$$

Here $H(x, y)$ is the depth of the mixed layer base, ∇ the gradient operator, u_{H} the horizontal velocity vector, and w_{H} the vertical velocity at the base of the mixed layer. In practice all these contributions to the subduction are calculated using mean climatological data. The mixed-layer topography is that of late winter, when the mixed-layer depth is the largest, the horizontal velocities are calculated as geostrophic currents using a deep reference level and the Ekman pumping velocity is determined from mean wind-stress fields. This approach does not take the role of synoptic-scale and time varying structures like eddies into account, which in the analysis of model data have shown to also

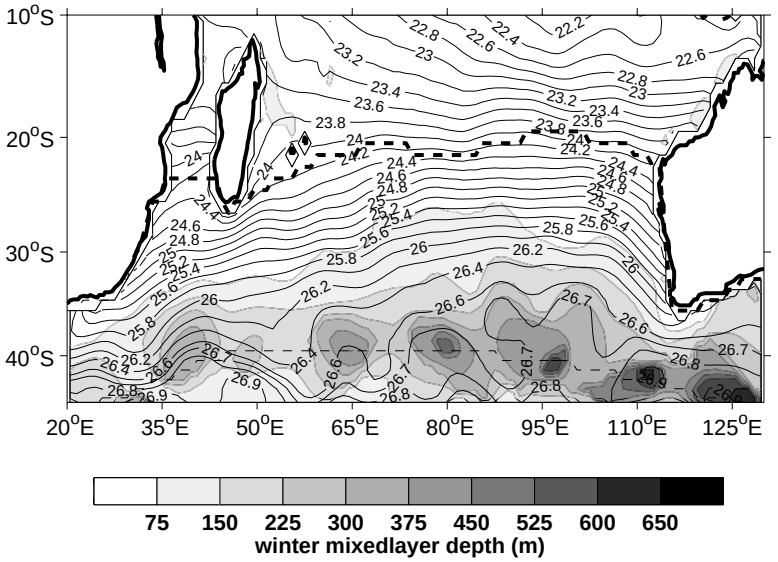

Fig. 1. Depth (shading) and density of the deepest Southern Hemisphere winter mixed-layer depth as calculated from the WOA 98 data using the 0.125 kg m^{-3} criterion. The broken lines indicate the boundary of the ventilating region. In the south it is given by the trough of the deepest mixed layer during winter, and in the north by line of the annual mean surface density 23.5 kg m^{-3} (see text for details).

contribute to the subduction. We will come back to this issue later.

A second method to estimate subduction rates is the "water age approach", proposed by Jenkins (1987), that uses vertical water age gradients calculated for example from geochemical tracer data. Geostrophy and conservation of potential vorticity are assumed. Following isopycnal surfaces the age of the water increases along the streamlines in the interior. If the baroclinic velocity shear is negligible and vertical diffusion is weak, and if the effect of horizontal diffusion on the tracer ages can be accounted for, a vertical age gradient in the interior will be observed that reflects the difference in time when the water parcels left the mixed layer. This age gradient ($\partial t/\partial z$) is proportional to the subduction rate, while a correction for the layer shrinking through conservation of potential vorticity is achieved through the relation of outcrop latitude (f_0) vs. observational latitude (f) (Williams et al., 1995). The "water-age approach" subduction rate can be written as

$$S_{\mathrm{ann}} = f_0/f(\partial t/\partial z)^{-1}. \quad (2)$$

An important difference between the kinematic and the water-age approach is their consideration of subduction forced by transient eddies. Using the kinematic approach on a climatological field, the eddy contribution is not considered, unless the eddies are stationary. In contrast, the water-age approach takes all contributing factors into account that transfer water into the interior. A comparison of the results from both approaches allows an estimate of the eddy contribution to the subduction.

The main water masses occupying the thermocline of the southern Indian Ocean are the Central Water and the subtropical and subantarctic Mode Waters (Sverdrup et al., 1942; McCartney, 1977, 1982). Minor contributions stem from the Red Sea and Arabian Gulf outflows and from the Pacific–Indian through flow. Central Water is characterised through a quasi-linear relationship in temperature and salinity (Sverdrup et al., 1942). Mode Waters have the same T–S characteristics as the lower part of the Central Water, but are limited to narrow density ranges (McCartney, 1977, 1982; Fine, 1993). Karstensen and Tomczak (1997) found a side-by-side existence of Mode and Central Waters in the southern Indian Ocean along 32°S. The Mode Waters observed off Australia were just 5 years old whereas the age of the Central Water was about 20–30 years. These age differences were attributed to different formation mechanisms: Central Water is transferred to the thermocline through Ekman pumping, while the Mode Water transfer has to be divided into two stages: the formation stage, where the water is homogenised to depths of several hundreds of meters through convection (England et al., 1993; Ribbe, 1999), and the injection stage, where the essentially lateral input into the thermocline occurs.

Until now only few attempts have been made to quantify thermocline subduction for the southern Indian Ocean hemisphere. Speer et al. (1995) found thermocline water formation of 20 Sv for densities > 25.0 kg m^{-3} by analysing surface flux data. Zhang and Talley (1998) found a formation based on a transformation of higher densities ($\sigma_\theta > 25.7$ kg m^{-3}), but of similar magnitude. Sloyan and Rintoul (2001) used an inverse model considering surface fluxes and diapycnal mixing. They found a formation of about 24 Sv between $\gamma = 26.0$ and 26.8 (which may be treated in the following as being similar to potential density) from surface fluxes. Along 32°S they found a northward transfer into the thermocline of about 34 Sv between 24.0 and 27.0 kg m^{-3}. Marsh et al. (2000) investigated southern ocean water-mass formation in a non-eddy resolving model with a parameterised bolus velocity and a seasonally varying surface forcing. In the Indian Sector south of about 25°S they found Subantarctic Mode Water formation of 20 Sv for the layer 26.52–26.80 kg m^{-3}, increasing to an overall formation of 25 Sv for the density range 25.28–27.03 kg m^{-3}. The role of the northward drift of surface waters from the Antarctic Circumpolar Current in the formation of Mode Water (and Intermediate Water) is controversial: Ribbe and Tomczak (1997) and later Ribbe (1999) found cross-frontal mixing to play a vital role in the formation using model results, while England et al. (1993) found no

evidence for an Antarctic contribution from there simulations.

In this study we will quantify the contributions from vertical Central Water and horizontal Mode Water ventilation by employing the kinematic approach. Error estimates for different choices of mixed layer depth criteria, reference level for the geostrophic calculation and the wind field will be given. We will then compare the combined ventilation rates with those obtained from the water age approach to estimate the contribution of transient eddies to the subduction. A comparison with water-mass formation rates as deduced from surface density fluxes is made. Finally comparisons with tracer characteristics in the interior of the subtropical gyre are made and the source water characteristics are deduced.

2. Subduction rate: kinematic approach

2.1. Mixed layer depths and outcrop region

The mixed layer plays a key role for the subduction. Its characteristics during late winter set the initial tracer values of the water masses ventilating the interior, its thickness has a direct influence on the reduction of the vertical Ekman pumping velocity, and the topography of its base controls the contribution of the horizontal flow to the subduction (Eq. (1)).

A density increase of $0.125\ \mathrm{kg\ m^{-3}}$ over the surface value is typically used as a criterion when calculating the mixed-layer depth from observational data. We will follow this somewhat arbitrary choice, but in a later section will explore the implications when using other criteria. The World Ocean Atlas 1998 (WOA 98) southern hemisphere winter temperature and the annual mean salinity data (Levitus and Boyer, 1994; Levitus et al., 1994) on a 1° latitude times longitude grid are used to calculate the mixed-layer depths. A comparison of the general patterns of monthly (September) and winter (July–September) temperature field revealed only minor differences, and we therefore used the winter data to overcome problems with sparse data distribution. For salinity seasonal changes are generally low in the depth range considered, which allows the use of annual mean rather than seasonal or monthly data.

On the large scale the winter mixed-layer base in the southern Indian Ocean increases from north to south, with the deepest depths found along the southern rim of the subtropical gyre around 40°S (Fig. 1). In the southern half of the gyre depths increase also towards the east, reflecting the heat loss of the ocean to the atmosphere which leads to a successive deepening of the mixed layer along streamlines (England et al., 1993). The deepest mixed-layer depths are found in the south-east between 100°E and 130°E and south of 40°S between the subantarctic and subtropical fronts (Belkin and Gordon, 1996). In this longitude range Karstensen and Tomczak (1997) found the youngest Mode Water along the 32°S section.

To quantify the overall subduction rate, the extent of the outcrop region from where the gyre is ventilated has to be determined. This can be done by looking at the seasonal cycle of the mixed-layer depth. Water irretrievably entering the thermocline originates from the deepest and thus densest mixed layer in late winter/early spring. Water parcels subducted during the rest of the year are always re-entrained into the mixed layer when it deepens during the cooling season (Stommel, 1979; Woods, 1985). A natural southern boundary for the ventilation region is therefore the trough in the deepest (winter) mixed-layer depth (Fig. 1). All water leaving the mixed layer further south has to pass this mixed-layer trough before it can reach the interior of the Indian Ocean subtropical gyre. Thus all calculated contributions from south of the trough could be ignored, as they are not relevant for the gyre ventilation.

The northern limit of the ventilation region has to be seen as the boundary between the outcrops of the relatively stable and shallow tropical thermocline at low latitudes and the permanent thermocline. From the analysis of surface flux data Speer et al. (1995) and Zhang and Talley (1998) found that water-mass formation occurs only for annual mean surface densities larger than $23.5\ \mathrm{kg\ m^{-3}}$. This surface density coincides with the line of zero wind stress curl (Hellerman and

Rosenstein, 1983), and we chose it as northern ventilation limit.

2.2. The vertical component: Ekman pumping

The rotation of the wind field through Ekman pumping drives the vertical component of the transfer of water into the thermocline. The vertical velocity w_H at the base of the mixed layer is given by the Ekman pumping velocity at the surface corrected for the contribution to the Sverdrup circulation within the mixed layer itself (Williams, 1991)

$$w_H = 1/\rho \,\mathrm{curl}\, T/f - \beta/f \int v \,\mathrm{d}z. \quad (3)$$

Here ρ is the density of the water, T the wind stress, β the meridional derivative of the Coriolis parameter (f), and v the meridional geostrophic velocity in the mixed layer.

For the calculation of the Ekman pumping velocity we used the Hellerman and Rosenstein (1983) wind-stress climatology, reduced by 20%, as suggested by Qiu and Huang (1995), to correct for shortcomings in parameterisations. Results from the use of other climatologies are discussed in a later section. The magnitude of the annual mean Ekman pumping velocity lies between 25 and 50 m yr^{-1} in the central and southern subtropical gyre (Fig. 2a). Within the ventilating region there are no particular strong horizontal structures. The line of maximum wind stress curl lies around 25°S with the highest values found off southwest Australia.

To determine the correction due to the Sverdrup transport, the velocity field in the mixed layer was calculated from the thermal wind equation using annual mean temperature and salinity values from the WOA 98 hydrographic data set base (Marshall et al., 1993). A zero velocity reference level of 2000 m, or at the sea floor in shallower regions, was used. This reference level roughly coincides with the depth range deduced from tracer data by Stramma and Lutjeharms (1997) to calculate the

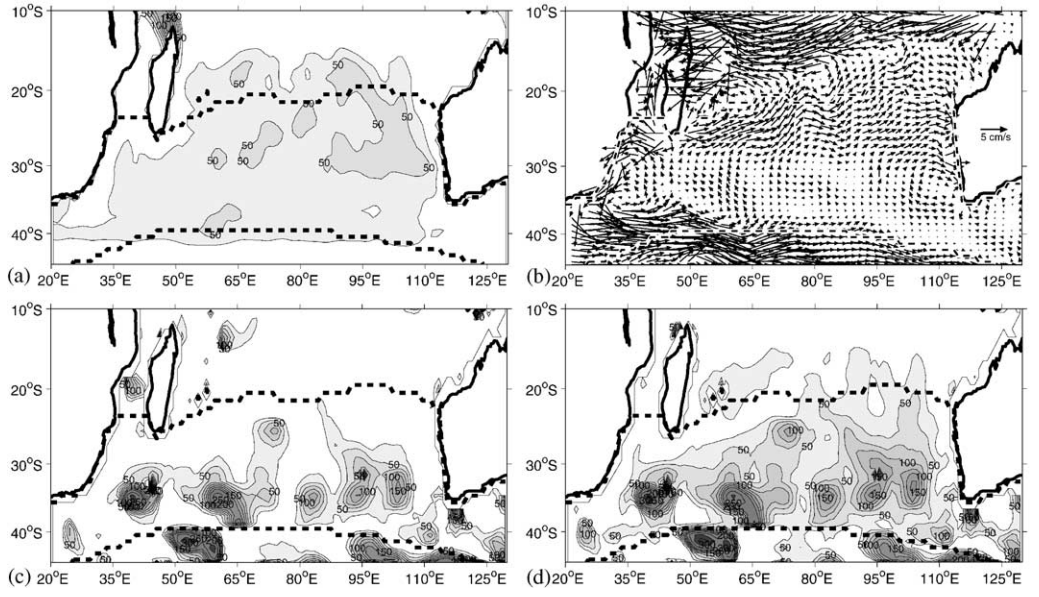

Fig. 2. (a) Ekman pumping velocity calculated from a 20% reduced version of Hellerman and Rosenstein (1983) wind stress data, (b) geostrophic velocity field at the base of the mixed layer, calculated from the WOA 98 data, using 2000 m depth as a level of no motion, (c) Meridional lateral component of the subduction rate, (d) annual mean subduction rate (lateral input based on meridional component only). Units are m yr^{-1}.

mean flow field of the Indian Ocean subtropical gyre. The overall reduction of Ekman pumping is marginal and substantial local reductions only in regions of strong northward currents, as north of Madagascar.

2.3. The horizontal component

The horizontal velocity field contributes to the subduction in regions where the base of the mixed layer is inclined to the horizontal plane (Eq. (1)). This topography is steepest near the trough of high mixed-layer depths, both in the meridional and in the zonal directions (Fig. 1). The individual depressions cannot be linked to features in the topography of the ocean floor, but instead seems to be a combined result of poor data coverage and the gridding procedure in the WOA 98 data set (Lozier et al., 1994). The flow field in the ventilating area is dominated by the Agulhas retroflection in the southwest corner of the gyre (Fig. 2b). Further to the east current velocities decrease, but the eastward-flowing South Indian Ocean current (Stramma, 1992) is visible along the entire ocean at about 40°S. The subtropical gyre circulation is centred at about 25°S, well north of the ventilating region. Along the Australian coast a southward flow, associated with the Leeuwin Current (Cresswell and Golding, 1980) is visible.

We split the lateral component of the subduction into a meridional (north/southward) and a zonal (east/westward) part and count the positive and the negative contributions separately. These are summarised in Table 1. Which of these four contributions now ventilates the thermocline? The positive components by definition give the transfer of water from the mixed layer into the thermocline, whereas the negative parts are not directly related to the transfer from the thermocline into the mixed layer (see Qiu and Huang, 1995, for a detailed discussion). We here discuss both numbers in terms of their general plausibility. The magnitude of the meridional component (either positive or negative) reflects the equatorward rise of the mixed-layer base. Transports are about 17 Sv northward into the thermocline of the subtropical gyre. The −4 Sv are most likely caused by irregularities in the mixed-layer base of the gridded data set. The zonal components reflect the general eastward deepening of the mixed-layer base with twice as large negative than positive rates. Here, the positive numbers (effective subduction), however, may not indicate an irretrievable input into the thermocline, but rather simply reflect the bumpy structure within the mixed-layer trough. Shallow ridges in the topography in an eastward flow are associated with strong subduction on the upstream side, but also with negative fluxes on the downstream side. Fluxes associated with errors in the mixed-layer topography thus simply cancel out, and the overall integrated fluxes should be correct. Part of this water should participate in the transformation into Mode Waters and can be recycled into the thermocline.

Table 1
Subduction of water from the mixed layer into the permanent thermocline of the southern Indian Ocean, calculated with the kinematic method. The second column (standard) gives the transport in Sv (1 Sv = 10^6 m^3 s^{-1}) for the different components in Eq. (1), northward transfer only. The maximum deviation from these values for different mixed-layer criteria, wind fields and reference levels are shown in the three right columns. H&R: Hellerman and Rosenstein (1983) windfield; SOC: Josey et al. (1999) climatology

	Standard (0.125 kg m^{-3}, 80% H&R, 2000 m)	Winds (SOC, 100% H&R)	Mixed layer (0.075 kg m^{-3}, 0.200 kg m^{-3})	Refernce level (1750 m, 2500 m)
$+u\ \mathrm{d}H/\mathrm{d}x$	10.4	2.2	0	0.6
$\mathbf{+v\ dH/dy}$	**17.6**	**3.2**	0	**0.9**
$-u\ \mathrm{d}H/\mathrm{d}x$	−18.6	2.6	0	0.7
$-v\ \mathrm{d}H/\mathrm{d}y$	−3.8	0.9	0	0.3
W_{Ekm}	20.8	0	5.2	0
$\boldsymbol{W_{\mathrm{H}}}$	**16.7**	**0.1**	**5.1**	0

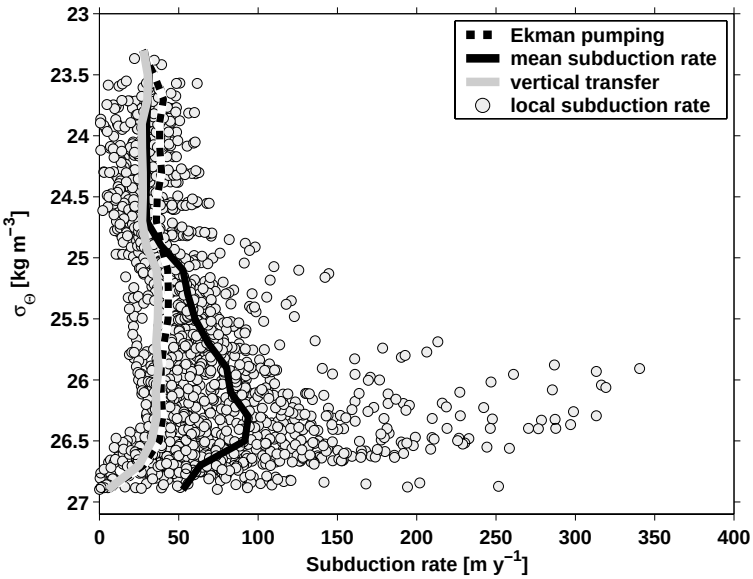

Fig. 3. Subduction rates of the individual 1° latitude times longitude boxes vs. density of the subducted water (dots), calculated with the kinematic approach (standard case, see Table 1). Mean in 0.1 kg m^{-3} density increments of local subduction rates (black line), vertical transfer (grey line) and Ekman pumping (broken line). At low densities the Ekman pumping contributes almost all water to the subduction while at higher densities the lateral input dominates. Only the northward lateral component are used.

However, to ensure that the water is irretrievable transferred into the thermocline we consider in the following only the positive northward component of 17 Sv and the vertical contribution of 17 Sv, the corrected Ekman pumping. This gives an overall subduction of 34 Sv into the thermocline of the Indian Ocean. The regional distribution of this subduction is shown in Fig. 2d, which in the south reflects largely the structure of the mixed-layer depth (Fig. 1). Largest rates occur along the deepest mixed-layer trough in the south, associated with lateral input. In the northern part of the subducting zone the vertical component becomes dominant. This shows up more clearly when looking at the rates with respect to the density of the subducted water (Fig. 3). In the less dense water range (<25.2 kg m^{-3}) Ekman pumping drives the subduction, while towards higher densities the lateral input increases and dominates. The largest input can be found in the density range between 25.2 and 26.85 kg m^{-3}. It should be stressed that the scatter around the mean subduction rate in Fig. 3 is due to the spatial variability of the rates and does not reflect uncertainties in the calculations.

2.4. Uncertainties

The above calculations are based on a number of assumptions that include the criterion for the mixed-layer depth, the level of zero velocity for the geostrophic calculations and the choice of the wind field. For the standard case we have taken values of 0.125 kg m^{-3}, 2000 m and used the Hellerman and Rosenstein winds in the 20% reduced version. We have repeated the calculations using different values and using the original (100%) Hellerman and Rosenstein winds and "SOC global air–sea heat and momentum flux climatology" (Josey et al., 1999). The results are summarised in Table 1.

Using a different mixed-layer base density has the largest impact on the northward lateral subduction rate and leads to a change of about

20%. The effect is due to the sensitivity of the fluxes to the shape of the mixed-layer topography, which is probably the most crucial uncertainty in this exercise. Using the 100% Hellerman and Rosenstein winds increases the vertical fluxes by 25%, which really does not come as a surprise, as the fluxes and the curl of the wind stress are linearly related. Using different reference velocities for the geostrophic calculations causes the smallest change in the fluxes.

3. Subduction rate: water-age approach

As a second, independent estimate we calculated the subduction rates using the water age approach (Eq. (2)). A comparison between the rates from both approaches may allow to judge whether transient eddies contribute strongly to the subduction or not.

The distribution of tracer data for a calculation of water mass ages in the southern Indian Ocean is even sparser than that of traditional hydrographic data. In particular only data within the gyre can be used (south of 17°S), preventing age changes due to mixing with water from the Pacific-Indian through flow and from the north. Here we calculate the vertical age gradient ($\partial t/\partial z$) in the interior of the subtropical gyre from CFC apparent ages along two zonal "World Ocean Circulation Experiment" (WOCE) sections (I5 and I3, see map in Fig. 8) and three meridional section (I5 along 80°E, see McCarthy et al., 1997; I8 along 95°E and I9 along 115°E, see Hufford et al., 1997). The zonal sections cut the subtropical gyre, while the meridional ones cut the region where Mode Water formation is known to occur. Age determination was done in the usual manner by transferring each measured CFC value into an apparent atmospheric value, using the solubility function of Warner and Weiss (1985), assuming 100% saturation, and comparing it with the atmospheric time history of the CFC component (Walker et al., 2000). The mean outcrop latitude (f_0) was determined through a polynomial fit on winter outcrop densities calculated from the WOA 98 data (see Fig. 1, contours). The non-zonal orientation of the isopycnals will be discussed later as one potential error source for the calculated rates. Furthermore, the influence of lateral mixing on the apparent ages was corrected using the age error map of Karstensen and Tomczak (1998, their Fig. 7). In general CFC-12 and CFC-11 ages are affected in the order of 10% towards younger ages.

After having corrected the ages for lateral mixing effects, upper and lower bounds for the subduction rates were calculated for each data point, using the r.m.s. scatter of the outcrop density/latitude fit. The subduction rates from the water age approach are linked to individual water parcels in the interior of the thermocline rather then to a subduction location, as in the case with the kinematic approach. This means that the volumes of subducted water can only be estimated if the particle trajectories are known (O'Connor et al., 1998). These, however, cannot be calculated from in situ hydrological data only.

What we can do is to compare rates from both approaches with respect to the outcrop densities (Fig. 4). The scatter between the individual estimates is as large as it is for the local rates of the kinematic approach (Fig. 3), but its overall distribution is similar. In both cases the largest subduction rates occur in the density range between 25.2 and 26.85 kg m^{-3}. A quantitative comparison of the two estimates is more difficult to achieve. It is not clear that the individual tracer data from the sections in the interior cover the thermocline waters from all subduction regions in a representative manner. Some regions, like the areas of Mode Water formation may be oversampled, while others, in the quieter interior, may be not represented in a statistically satisfactory way. Also, the number of observational points in the low-density range is rather low.

Instead of using a simple average of the subduction rates in the different density classes, as done for the results of the kinematic computations (Fig. 3), we have therefore in the case of the tracer results plotted the median value of the subduction rates (Fig. 4). If the data distribution is Gaussian, mean and median show the same value, but for a skewed distribution as for the tracer derived subduction rates, the median is more appropriate.

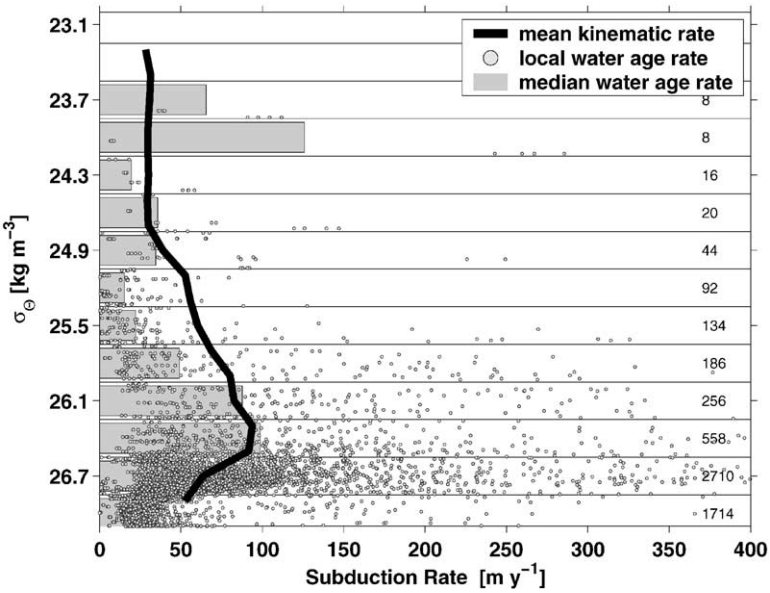

Fig. 4. Subduction rates vs. density as calculated with the water age approach. Data are from the zonal WOCE sections I3 (18°S) and I5 (32°S) and from the meridional sections I5 (80°E), I8 (95°E) and I9 (115°E). Data with an apparent oxygen utilisation less the 10 μmol kg^{-1} are excluded. The bar graph is the median rate in 0.3 kg m^{-3} density bins, the numbers on the right give the number of points in a bin. The black line indicates the mean subduction rate as calculated from the kinematic approach (see Fig. 3).

Comparing now the mean and median rates of both approaches (line and bars in Fig. 4) gives an excellent agreement in the dense water range, whereas for densities between 25.0 and 26.0 kg m^{-3} the water age rates are only about half. In the very low density range below 24.0 kg m^{-3} water age rates are much higher. This means that in regions or layers with good data coverage the agreement between the two methods is good, in our case this agreement covers the range of Mode Water masses. These regions are characterised by a high lateral input and, because they are frontal regions, the existence of meso-scale eddies is likely. However, the close agreement between the two independently estimated subduction rates now show that the eddy contribution must be small if not negligible.

We further tested the potential importance of eddies by increasing the (northward) lateral component with random noise of 15 m yr^{-1} (median of the lateral component). The result is an increase of 25% on the lateral input and an overall increase of about 10%.

4. Water-mass transformations and spreading

The water-mass transfer in the interior of the ocean has to be balanced through buoyancy fluxes at the air–sea interface. Using the SOC climatology we calculated density fluxes for the Indian Ocean (Fig. 5). Annual mean water-mass formation sites are seen in the subtropics west of Australia and in the southwest along the Agulhas Retroflection.

Following the method of Tziperman (1986) and Speer and Tziperman (1992), the monthly air–sea surface density fluxes are integrated over surface density bins ($\Delta\sigma_\theta = 0.2$ kg m^{-3}) and time to derive annual mean water-mass transformation rates (Fig. 6). Essentially, each number gives the annual mean flux of water through a density surface driven by air–sea fluxes of heat and freshwater. A

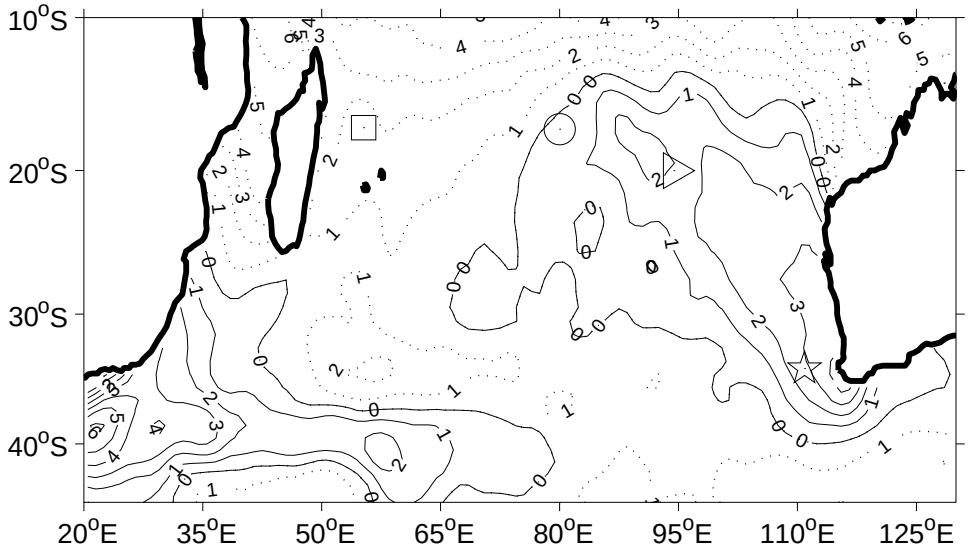

Fig. 5. Annual mean surface density flux (10^{-6} kg m^{-2} s^{-1}) estimated from the SOC climatology. Markers indicate positions of CTD stations used in Fig. 7.

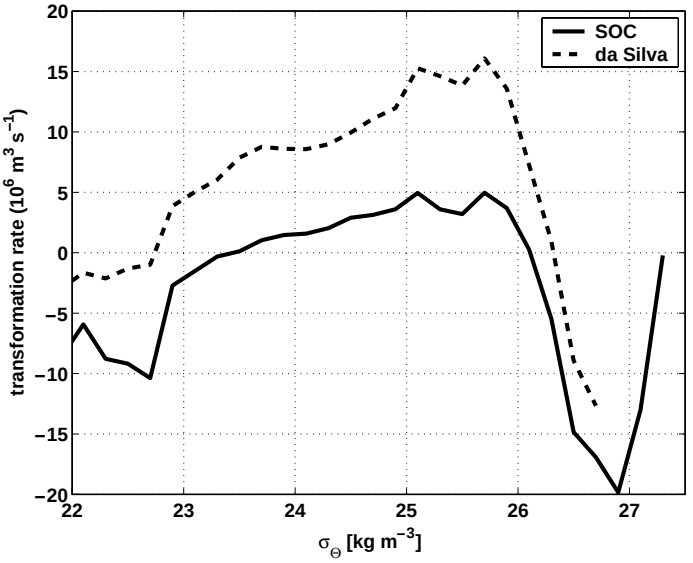

Fig. 6. Water-mass transformation rates (Sv) calculated from the SOC (Josey et al., 1999) and from da Silva et al. (1994) climatologies of sea surface density fluxes analysed in 0.2 kg m^{-3} density bins south of 5°S between 20°E and 120°E.

positive number stands for the transfer of water to larger densities (see Tziperman, 1986 for details). The SOC climatology is not in a global equilibrium and the ocean gains heat in the order of 30 W m^{-2} (Josey et al., 1999). Thus, the magnitude as well as the pattern of the fluxes is different

from earlier investigations (Zhang and Talley, 1998: compare with there Fig. 4a) based on globally "constrained" fluxes (da Silva et al., 1994). However, on local scales the SOC climatology was found to be in agreement with independent observations (Josey et al., 1999; Joesy, 2001).

In the following we use both the SOC and the "constrained" density flux as given by da Silva et al. (1994) for our estimates. In both climatologies water-mass formation occurs in the density range from about 23.5 to 26.6 kg m^{-3} (Fig. 6). Ignoring mixing and inflow from boundaries, the overall water-mass formation for a density range is the total difference between the transformation rates over that range (Tziperman, 1986). Thus the SOC climatology gives about 25 Sv, composed of a transformation of about 5 Sv of water <26.0 kg m^{-3} to denser water and 20 Sv by transferring dense water into less dense water. The corrected da Silva et al. climatology gives, in the density range resolved, about 28 Sv composed from 16 Sv less dense to denser water and 12 Sv vice versa. (Note that earlier water mass studies for the Indian Ocean, e.g. Zhang and Talley, 1998, did not have a transformation towards less dense water.) Sloyan and Rintoul (2001) used an ocean inverse model initialised with climatological air–sea fluxes and found an overall transformation of water between 26.0 and 26.8 kg m^{-3} of about 24 Sv with equal less dense to dense and vice versa conversion which compares well with our estimate of 23 Sv for this density range.

The formation in both climatologies supports in general our estimate from interior data of about 34 Sv. However, if Mode Water formation is seen as a transformation of surface water south of the subantarctic front (Ribbe and Tomczak, 1997), the SOC climatology with the larger transformation of denser water to less dense is doing a better job. As we will see later, the signature of water from Antarctic origin is evident in the outcrop tracer distribution as well.

The pattern of the annual mean surface buoyancy flux from both climatology leads to a second consequence in terms of the interior salt fluxes. Schmitt et al. (1989) suggested that a haline density flux into the ocean drives interior salt finger fluxes. Under the condition that the fluxes at the upper and lower boundaries are zero, Schmitt (1981) predicted a rotation of the T/S curve with time (Fig. 7, left) using a vertical mixing model with different diffusivities for temperature and

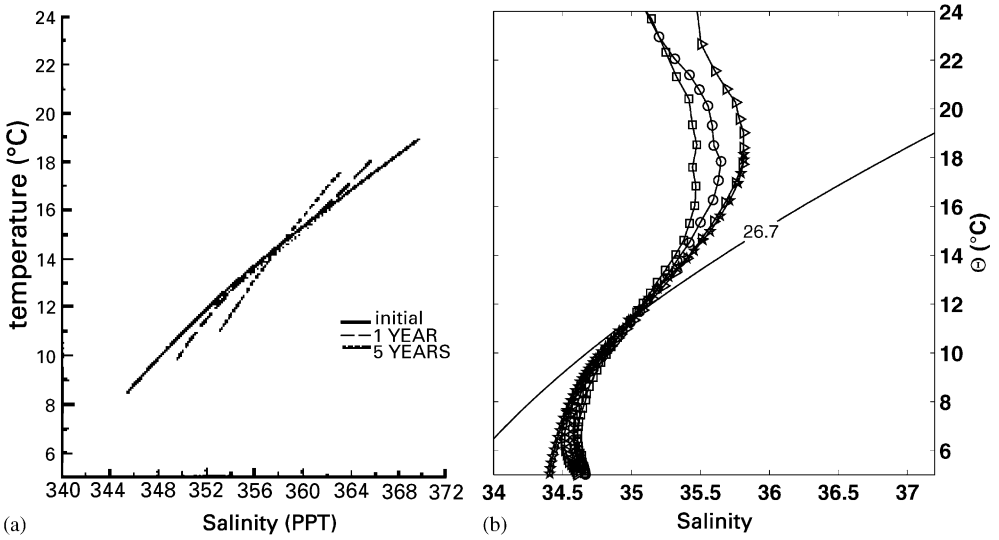

Fig. 7. Rotation of the T/S curve due to salt finger type double diffusion. Left: No flux model (reproduced from Schmitt, 1981). Right: CTD data from recent WOCE cruises (see Fig. 5 for station positions).

salinity. In order to be effective, the haline component of the density flux into the ocean must be accompanied by a total (haline and thermal) flux. In the Indian Ocean subtropical gyre such conditions are present west of about 80°E (Fig. 5). Average CTD profiles from WOCE surveys at different points in the interior of the gyre do indeed show a similar rotation of the T/S curve (Fig. 7, right, for positions see Fig. 5) as predicted by Schmitt (1981). This underlines the importance of double diffusive processes in the transformation of thermocline waters. It should be noted that the rotation point is on the 26.7 kg m^{-3} isopycnal, identified by You and Tomczak (1993) as the lateral spreading surface of the Indian thermocline. Our observations indicate that this is questionable, because salt–finger salt fluxes are diapycnal fluxes, even if the T/S relation looks like it is not altered.

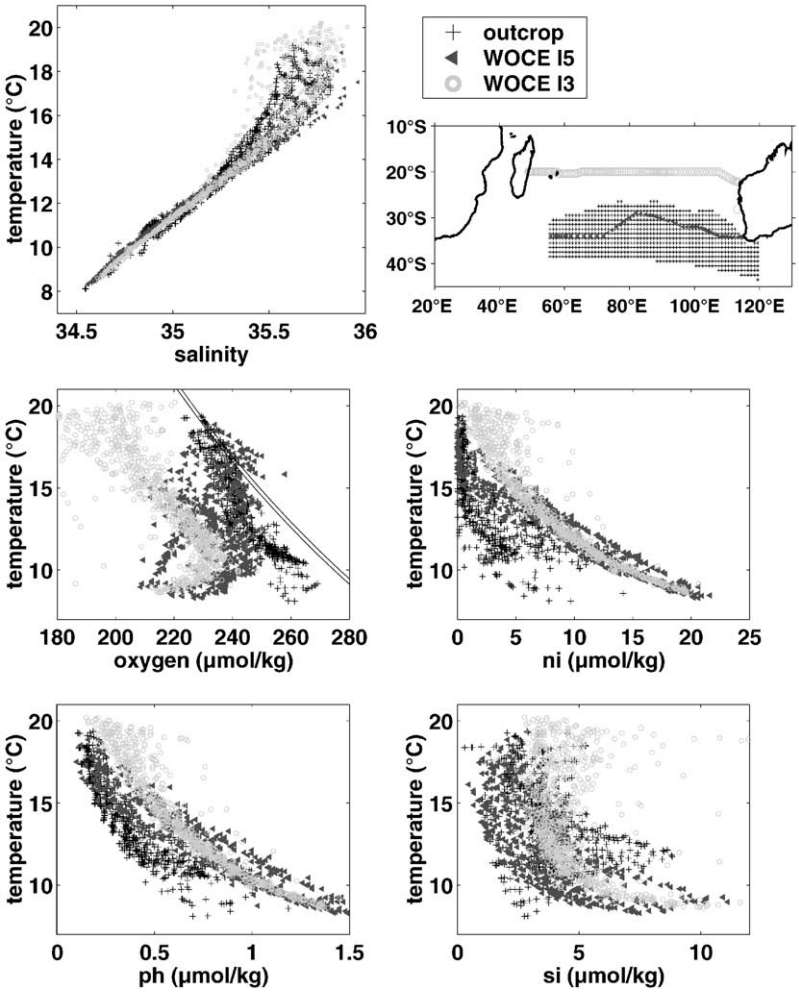

Fig. 8. Comparison of tracer characteristics for data from the base of the winter mixed layer from WOA 98 data (temperature $<20°C$) in comparison with observational data along WOCE section I5 (32°S) and I3 (18°S). See map for winter outcrop surface and station positions. (upper) Temperature/salinity diagram (middle), oxygen/temperature and nitrate/temperature, and (lower) phosphate/temperature and silicate/temperature.

5. Water-mass characteristics

In the context of tracer and biogeochemical cycling studies end-members of unmixed water masses are widely used for water mass analysis. These end-members are often obtained in a heuristic way by plotting observational data and identifying vertexes composing the interior field subjectively. Other tools using statistical methods include cluster analysis (e.g., You and Tomczak, 1993). The deduced values always depend on the distribution and quality of the underlying data and may not reflect the initial or pre-formed end-members. In particular for water masses covering a T/S range rather then a point the upper and lower boundaries (say in temperature) are difficult to determine.

Such limitations of heuristic methods can be overcome when the underlying physical processes of the water-mass formation are considered explicitly. Here we will use the characteristics of tracers at the base of the winter mixed layer in the outcrop region and define the water masses present in the ventilated thermocline in terms of upper and lower source waters. Although ventilation occurs up to temperatures of about 26°C, we used 20°C, the temperature of the salinity maximum, as the upper source water, thereby following the "classical" Central Water definition of Sverdrup et al. (1942). The water above > 20°C is usually referred to as Subtropical Underwater. The Underwater characteristics reflect the equatorward decrease in surface salinity. The associated interior salinity stratification does not support double diffusive salt-finger fluxes, which would smooth out salinity anomalies (Schmitt, 1981); the scatter here is much larger than for the Central Water itself.

Table 2
Source water characteristics for the Indian Ocean Central Water as analysed from the property distribution along the winter outcropping using WOA 98 data

Parameter	Upper	Middle	Lower
Temperature (°C)	20	13	9
Salinity	36.00	35.25	34.65
Oxygen (μmol kg^{-1})	227	244	268
Phosphate (μmol kg^{-1})	0.10	0.35	0.85
Nitrate (μmol kg^{-1})	0	1	7
Silicate (μmol kg^{-1})	2.5	2.5	2.5

A comparison between outcrop characteristics and observational data along the two zonal WOCE section (I5 at 32°S and I3 at 18°S) shows good agreement in their temperature and salinity characteristics (Fig. 8). Scatter towards lower salinity values is due to Pacific–Indian through flow water transferred along the western flank of the subtropical gyre. Thus, for defining the source

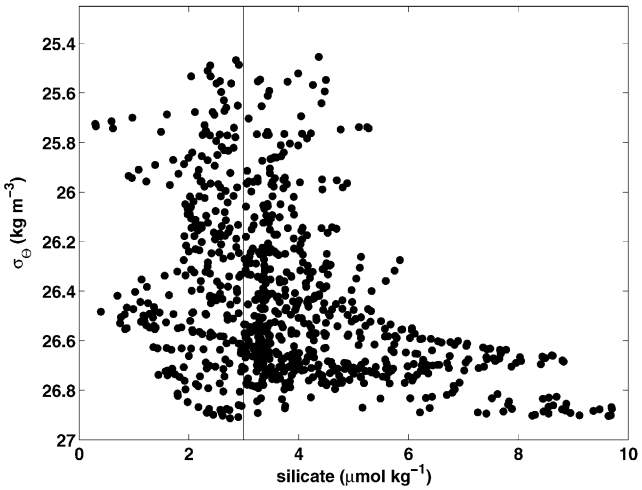

Fig. 9. Silicate/density relation at the base of the winter mixed layer in the subduction area.

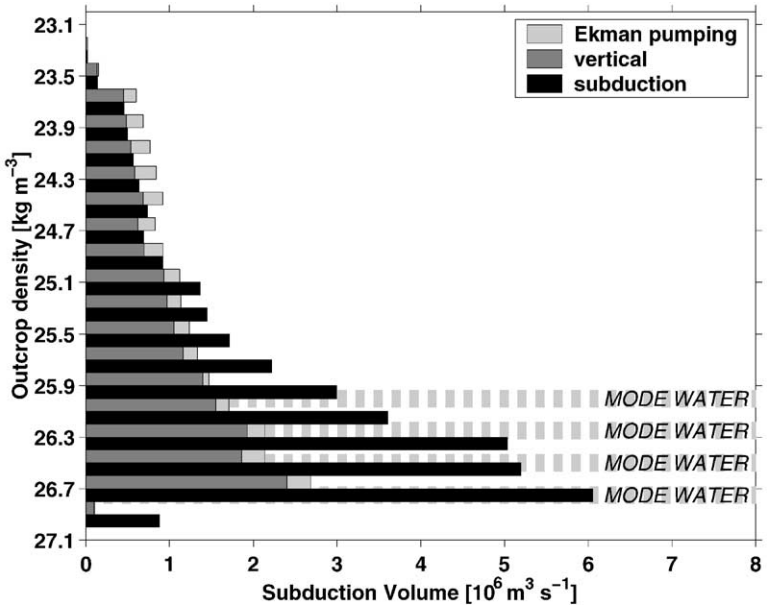

Fig. 10. Volume transfer of water into the Indian Ocean thermocline in terms of the winter outcrop density. The transport is separated into the Ekman pumping (with overlaid effective vertical transport) and the transport as calculated from the annual mean subduction rate (northward lateral component only). Mode Water densities as given by Fine (1993) are indicated by light grey broken lines.

water values we used only data east of 55°E to minimise this effect. WOCE I5 section along 32°S crosses the formation region.

The salinity distribution along I5 within the upper temperature range shows larger scatter when compared to WOCE I3 (Fig. 8). This indicates that the salt-finger fluxes have not yet effectively stabilised the T/S curve within the newly formed waters. In the upper water ($T > 15$°C) (over) saturation in oxygen, nearly no nitrate, and a pre-formed phosphate concentration can be found (Fig. 8). Nutrient data along I3 are already affected by re-mineralisation of organic matter and the accompanied oxygen consumption. In the temperature range <10°C the increase in scatter in the outcrop characteristic may be associated with the change in the underlying data from winter to annual mean (for phosphate, nitrate, and silicate only). Comparing oxygen along outcrop and I3, a change in the rate of oxygen consumption (re-mineralisation) with depth is evident. In the lower temperature range (<14°C) the outcrop oxygen is under-saturated by about 10 μmol kg^{-1}, indicating a time delay between the convective formation of Mode Water and the transfer into the thermocline via the lateral component of subduction.

Exchange of water over the Subantarctic front is in particular clear in the outcrop silicate data (Fig. 9) where at the Mode Water densities silicate concentrations show large scatter. Concentrations of nitrate and oxygen in the waters of southern origin are locally being "reset" through air–sea interaction processes, while silicate is not affected in the same matter. This is consistent with the findings of a northward drift of water cross the Antarctic Circumpolar Current and subsequent sinking in the convection region as suggested by Ribbe and Tomczak (1997). Source water definition values for the subducted water deduced from the property plots are summarised in Table 2.

6. Conclusions

We used the WOA 98 hydrographic data climatology to calculate subduction rates and

volumes for the permanent thermocline of the Indian Ocean. Using the kinematic approach provides a detailed inventory of the subducted water masses, both in terms of the density distribution (Fig. 10) and in terms of the regional distribution (Fig. 2d). It turned out that in the southern Indian Ocean subduction of 34 Sv is composed from equal amounts of northward lateral and vertical, essentially Ekman pumping, subduction. In the density range > 25.2 kg m^{-3} the lateral component dominates by 50% over the vertical corresponding to the range of Mode Waters (McCartney, 1977, 1982; Fine, 1993).

The overall transfer supports findings of Sloyan and Rintoul (2001), who found about 34 Sv of northward transfer for their layers 8–12 (density of about 25.0–27.0 kg m^{-3}). The similarity confirms our approach to consider only the northward component as contributing to the ventilation of the gyre. Moreover, the estimated transport between 25.7 and 26.8 kg m^{-3} is in good agreement with those derived from surface fluxes (20 and 26 Sv) and further supported by the recent calculation of 25 Sv between 25.28 and 27.03 kg m^{-3} by Marsh et al. (2000) using a southern ocean intermediate resolution OGCM.

Comparisons with rates derived from an age tracer approach compared well on a local scale. For high densities, i.e. in the Mode water range, the rates are in good agreement. For lower densities the tracer data are much sparser and the associated poorer statistics lead to a larger deviation from the results of the kinematic approach. One also has to keep in mind that the horizontal coverage of the subtropical gyre with tracer data is far from satisfactory. However, the agreement between these estimates based on different methods over most of the density range allow us to conclude that the overall effect of transient eddies on setting the transfer is not dominant.

The subduction into the Indian Ocean is somewhat different to that in the Northern Hemisphere Atlantic and Pacific Oceans, where the Ekman pumping dominates the subduction by a factor of two over the lateral intrusions (Qiu and Huang, 1995). Why is this so? The reason may be found both in the geometry of the ocean basins as well as in the pattern of the large scale circulation and the associated distribution of water masses and fronts. In the Southern Ocean there is a zonal current system associated with strong fronts that separate the subtropical gyre from the circumpolar current system. These fronts are associated with deep Mode Water formation mixed-layer depths reach more than 600 m, and the topography of the mixed-layer base is very steep. In contrast, the Mode waters in the North Pacific stem from depths of less than 200 m and are distributed in a wide pool rather than along a narrow trough (Huang and Qiu, 1994). Consequently the topography of the mixed-layer base is much less steep, leading to much weaker lateral subduction.

Tracer distributions along the deepest mixed-layer base allowed us to define the source water properties for the ventilating water masses. We identified Subtropical Underwater and Central Water to be injected from the vertical component (essentially Ekman pumping) while Mode Waters are associated with the lateral input. This can be seen clearly in the silicate distribution (Fig. 9). Central Water is transferred over the whole density range and as seen from an preformed value of about 3 μmol kg^{-1} while Mode Water densities have much larger values, suggesting an admixture of water of southern origin.

Acknowledgements

We acknowledge the helpful comments of three anonymous reviewer and from M. Visbeck. Financial support for this study was provided by the Bundesminister für Bildung, Wissenschaft Forschung und Technologie under the German WOCE programme.

References

Belkin, I., Gordon, A., 1996. Southern Ocean fronts from Greenwich Meridian to Tasmania. Journal of Geophysical Research (Oceans) 101, 3675–3696.

Bower, A.S., Hunt, H.D., Price, J.F., 2000. Character and dynamics of the Red Sea and Persian Gulf outflows. Journal of Geophysical Research (Oceans) 105, 6387–6414.

Cresswell, G.R., Golding, T.J., 1980. Observations of a south-flowing current in the south-eastern Indian Ocean. Deep-Sea Research I 27, 449–466.

Cushman-Roisin, B., 1987. Dynamics of the oceanic surface mixed layer. (Chap. Subduction), Hawaiian Winter. Workshop Proceedings, University of Hawaii at Manoa, Hawaii, USA, pp. 181–196.

da Silva, A.M., Young, C.C., Levitus, S., 1994. Atlas of surface marine data 1994. Vol. 3, Anomalies of heat and momentum fluxes; Vol. 4, Anomalies of freshwater fluxes, NOAA Atlas, NESDIS 4, 413pp.

England, M.H., Godfrey, J.S., Hirst, A.C., Tomczak, M., 1993. The mechanism for Antarctic Intermediate Water renewal in a world ocean model. Journal of Physical Oceanography 23, 1553–1560.

Fine, R.A., 1993. Circulation of Antarctic Intermediate Water in the South Indian Ocean. Deep-Sea Research I 40, 2021–2042.

Gordon, A.L., Ma, S., Olson, D.B., Ffield, A., Hacker, P., Talley, L.D., Wilson, D., Baringer, M., 1997. Advection and diffusion of Indonesian Throughflow Water within the Indian Ocean South Equatorial Current. Geophysical Research Letters 24, 2573–2576.

Hellerman, S., Rosenstein, M., 1983. Normal monthly wind stress over the world ocean with error estimates. Journal of Physical Oceanography 13, 1093–1104.

Huang, R.X., Qiu, B., 1994. Three-dimensional structure of the wind-driven circulation in the subtropical North Pacific. Journal of Physical Oceanography 24, 1608–1622.

Hufford, G.E., McCartney, M.S., Donohue, K.A., 1997. Northern boundary currents and adjacent recirculations off southwestern Australia. Geophysical Research Letters 24, 2797–2800.

Iselin, C.O.D., 1939. The influence of vertical and lateral turbulence on the characteristics of the waters at mid-depth. Transactions of the American Geophysical Union 20, 414–417.

Jenkins, W.J., 1987. ^{3}H and ^{3}He in the beta triangle: Observations of gyre ventilation and oxygen utilisation rates. Journal of Physical Oceanography 17, 763–783.

Josey, S.A., Kent, E.C., Taylor, P.K., 1999. New insights into the ocean heat budget closure problem from analysis of the SOC air–sea flux climatology. Journal of Climate 12, 2856–2880.

Joesy, S.A., 2001. A comparison of ECMWF, NCEP/NCAR and SOC Surface heat fluxes with moored buoy measurements in the subduction region of the North-East Atlantic. Journal of Climate 14 (18), 1780–1789.

Karstensen, J., Tomczak, M., 1997. Ventilation processes and water mass ages in thermocline of the southeast Indian Ocean. Geophysical Research Letters 24, 2777–2780.

Karstensen, J., Tomczak, M., 1998. Age determination of mixed water masses using CFC and oxygen data. Journal of Geophysical Research (Oceans) 103, 18599–18610.

Lozier, M.S., McCartney, M.S., Owens, W.B., 1994. Anomalous anomalies in averaged hydrographic data. Journal of Physical Oceanography 24, 2624–2638.

Levitus, S., Boyer, T., 1994. World Ocean Atlas, Vol. 4, Temperature. Technical report, NOAA Atlas NESDIS 4, US Gov. Printing Office, Washington, DC.

Levitus, S., Burgett, R., Boyer, T., 1994. World Ocean Atlas, Vol. 3, Salinity. Technical report, NOAA Atlas NESDIS 3, US Gov. Printing Office, Washington, DC.

Marsh, R., Nurser, A.J.G., Megann, A.P., New, A.L., 2000. Water mass transformation in the Southern Ocean of a global isopycnal co-ordinate GCM. Journal of Physical Oceanography 30, 1013–1045.

Marshall, D.P., 1997. Subduction of water masses in an eddying ocean. Journal of Marine Research 55, 201–222.

Marshall, J.C., Nurser, A.J.G., Williams, R.G., 1993. Inferring the subduction rate and period over the North Atlantic. Journal of Physical Oceanography 23, 1315–1329.

Marshall, J.C., Nurser, A.J.G., 1991. A continuously stratified thermocline model incorporating a mixed layer of variable thickness and density. Journal of Physical Oceanography 21, 1780–1792.

McCarthy, M.C., Talley, L.D., Bahringer, M.O., 1997. Deep upwelling and diffusivity in the southern Central Indian Basin. Geophysical Research Letters 24, 2801–2804.

McCartney, M.S., 1977. Subantarctic Mode Water. A voyage of discovery. Deep-Sea Research 24 (Suppl.), 103–119.

McCartney, M.S., 1982. The subtropical recirculation of Mode Waters. Journal of Marine Research 40, 427–464.

O'Connor, B.M., Fine, R.A., Maillet, K.A., Olson, D.B., 1998. The rate of formation of the subtropical underwater (STUW) in the north and south Pacific from drifter and tracer data. International WOCE Newsletter 31, 18–20.

Qiu, B., Huang, R.X., 1995. Ventilation of the North Atlantic and North Pacific: Subduction versus obduction. Journal of Physical Oceanography 25, 2374–2390.

Ribbe, J., 1999. On wind driven mid-latitude convection in ocean general circulation models. Tellus 51 (A), 517–525.

Ribbe, J., Tomczak, M., 1997. On convection and the formation of Subantarctic Mode Water in the Fine Resolution Antarctic Model (FRAM). Journal of Marine Systems 13, 137–154.

Schmitt, R.W., 1981. Form of the temperature–salinity relationship in the Central Water: Evidence for double-diffusive mixing. Journal of Physical Oceanography 11, 1015–1026.

Schmitt, R.W., Bogden, P.S., Dorman, C.E., 1989. Evaporation minus precipitation and density fluxes for the North Atlantic. Journal of Physical Oceanography 19, 1208–1221.

Sloyan, B.M., Rintoul, S.R., 2001. Circulation, renewal, and modification of Antarctic mode and intermediate water. Journal of Physical Oceanography 31, 1005–1030.

Speer, K.G., Tziperman, E., 1992. Rates of water mass formation in the North Atlantic Ocean. Journal of Physical Oceanography 22, 93–104.

Speer, K.G., Isemer, H.-J., Biastoch, A., 1995. Water Mass Formation from Revised COADS Data. Journal of Physical Oceanography 25, 2444–2457.

Stommel, H., 1979. Determination of water mass properties of water pumped down from the Ekman layer to the

geostrophic flow below. Proceedings of the National Academy of Science, USA, Vol. 76, pp. 3051–3055.
Stramma, L., 1992. The South Indian Ocean Current. Journal of Physical Oceanography 22, 412–430.
Stramma, L., Lutjeharms, J.R.E., 1997. The flow field of the subtropical gyre in the south Indian Ocean. Journal of Geophysical Research (Oceans) 102, 5513–5530.
Sverdrup, H.U., Johnson, M.W., Fleming, R.H., 1942. The oceans: Their physics, chemistry, and general biology. Prentice-Hall, Englewood Cliffs, NY, 1060pp.
Swallow, J.C., 1984. Some aspects of the physical oceanography of the Indian Ocean. Deep-Sea Research I 31, 639–650.
Tziperman, E., 1986. On the role of interior mixing and air–sea fluxes in determining the stratification and circulation of the oceans. Journal of Physical Oceanography 16, 680–693.
Warner, M.J., Weiss, R.F., 1985. Solubilities of chlorofluorocarbons 11 and 12 in water and seawater. Deep-Sea Research 32, 1485–1497.
Walker, S.J., Weiss, R.F., Salameh, P.K., 2000. Reconstructed histories of the annual mean atmospheric mole fractions for the halocarbons CFC-11, CFC-12, CFC-113 and carbon tetrachloride. Journal of Geophysical Research (Oceans) 105, 14285–14296.
Williams, R.G., 1991. The role of the mixed layer in setting the potential vorticity of the main thermocline. Journal of Physical Oceanography 21, 1802–1814.
Williams, R.G., Spall, M.A., Marshall, J.C., 1995. Does Stommel's mixed layer "demon" work? Journal of Physical Oceanography 25, 3089–3102.
Woods, J.D., 1985. In: Nihoul, J.C.J. (Ed.), Coupled Ocean–Atmosphere Models. Elsevier, Amsterdam, (Chapter 34: Physics of Thermocline Ventilation), pp. 543–590.
You, Y., Tomczak, M., 1993. Thermocline circulation and ventilation in the Indian Ocean derived from water mass analysis. Deep-Sea Research I 40, 13–56.
Zhang, H.-M., Talley, L.D., 1998. Heat and buoyancy budgets and mixing rates in the upper thermocline of Indian and Global Oceans. Journal of Physical Oceanography 28, 1961–1978.